Profile Control and its Effects on Plasma Confinement in Heliotron E

T. OBIKI, T. MIZUUCHI, F. SANO, H. OKADA, K. NAGASAKI, K. HANATANI, Y. IJIRI, T. SENJU, K. YAGUCHI, K. TOSHI, K. SAKAMOTO, T. HAMADA, H. FUNABA[1]
Institute of Advanced Energy, Kyoto University,
Uji, Japan.

K. KONDO, S. BESSHOU, H. ZUSHI[2], M. WAKATANI, Y. NAKAMURA, M. NAKASUGA
Graduate School of Energy Science, Kyoto University,
Uji, Japan.

V. V. CHECHKIN, V. S. VOITSENYA
Institute of Plasma Physics,
National Science Center "Kharkov Institute of Physics and Technology",
Kharkov, Ukraine.

K. IDA, S. SUDO, M. SATO, S. KOBAYASHI
National Institute for Fusion Science,
Toki, Japan.

H. SUGAI, H. TOYODA
Faculty of Engineering, Nagoya University,
Nagoya, Japan.

S. KADO[1], K. MURAOKA
Interdisciplinary Graduate School of Engineering Science, Kyushu University,
Kasuga, Japan.

K. MATSUO
Faculty of Engineering, Fukuoka Institute of Technology,
Fukuoka, Japan.

ABSTRACT

The effects of the plasma profile on the global energy confinement have been studied in Heliotron E with special regard to differences between heating methods (ECH, NBI, and NBI + ECH). With high power NBI, peaked T_i and peaked n_e profiles ($T_i(0)/\langle T_i\rangle \lesssim 2.7$, $n_e(0)/\langle n_e\rangle \lesssim 4.5$) were simultaneously achieved under low recycling conditions. A peaked n_e profile ($n_e(0)/\langle n_e\rangle \gtrsim 2.5$) could lead to the high T_i mode where the ion heat transport in the central region is substantially reduced. By changing the ECH launching condition (on-axis, off-axis and toroidally oblique injection), the peakedness of the T_e profile could be controlled in the range $1.3 \lesssim T_e(0)/\langle T_e\rangle \lesssim 4.5$. A peaked T_e- and flat n_e-profile ($3.5 \lesssim T_e(0)/\langle T_e\rangle$, $n_e(0)/\langle n_e\rangle \lesssim 1.8$) was brought about by the well focused on-axis ECH. The ECH plasma with a peaked T_e profile has higher stored energy than that with a moderately peaked T_e profile for the same injected ECH power and the same density region. The global energy confinement time normalized by the LHD scaling, τ_E^G/τ_E^{LHD}, showed $n_e(0)/\langle n_e\rangle$ dependence for the low T_i mode NBI plasmas. For the high T_i mode, the $n_e(0)/\langle n_e\rangle$ dependence of τ_E^G/τ_E^{LHD} was weak. These findings suggest that the LHD scaling should be modified to scale the global energy confinement of the helical plasmas in a wide range of $n_e(0)/\langle n_e\rangle$.

[1] National Institute for Fusion Science, Toki, Japan.
[2] Research Institute for Applied Mechanics, Kyushu University, Kasuga, Japan.

1. INTRODUCTION

For tokamaks, it is well known that the 'transport barrier', which is observed in the H mode or the reversed shear mode, locally builds up a sharp gradient of the pressure profile. In the Wendelstein 7-AS stellarator (W7-AS), narrowing of the density profile is observed during the transition to the optimum confinement state [1]. On the other hand, improved confinement states are sometimes achieved by plasma profile control in tokamaks, e.g. the PEP mode [2] or the supershot [3]. For heliotron/stellarator systems, there are also some reports discussing the effects of the density profile on the plasma performance. In Heliotron E, the peaked density profile produced by pellet injection could confine larger stored energy than in the case of fuelling by gas puffing in the moderate density region of NBI plasmas (2.5×10^{19} m^{-3} $\lesssim \bar{n}_e \lesssim$ 5.4×10^{19} m^{-3}) [4, 5]. The high T_i mode is observed with a peaked density profile under the low recycling conditions in Heliotron E [6, 7] and CHS [8]. The increase of a radial electric field E_r is considered an important factor for these improvements. There may be prerequisites for the initial density (or pressure) profile to trigger such E_r-development and they should be investigated. Once E_r increases to sufficient strength to cause transport improvement, a positive feedback loop for density peaking and E_r development will be established. From this point of view, profile control is important to the study of fusion plasma confinement.

In contrast to the case of density profile effects, there is scant experimental information about the effects of the temperature profile because the temperature profile is rather stiff (profile consistency) in tokamak L mode discharges. Recently, ECH has been applied not only for plasma production and heating but also for profile modulation, current drive and MHD control. To investigate (1) the controllability of the T_e profile and (2) the possibility of plasma current control in a heliotron configuration, perpendicular off-axis heating and oblique injection heating have been performed in Heliotron E by using a 106 GHz second harmonic ECH system [7]. It was shown that the T_e profile was sensitive to the single pass power absorption profile. In ECH plasmas, however, range over which the density profile can be varied is narrower than that in NBI plasmas. This is due to the strong particle pump-out phenomena. A certain amount of density profile control was, however, possible by changing the power absorption profile.

In this article, we report the controllability of density, temperature and pressure profiles through the use of ECH and NBI in Heliotron E under a boronized wall condition. The relation between the global energy confinement and the peaking parameters for n_e, T_e and T_i is discussed with special regard to the differences between heating methods. After a brief description of the experimental conditions in Section 2, the effects of the ECH power absorption profile on the electron temperature and density profiles are discussed in Section 3. The controllability of the density and temperature profiles for NBI (or NBI + ECH) plasmas and profile effects on the global energy confinement are discussed in Section 4. A summary is given in Section 5.

2. EXPERIMENTAL CONDITIONS

In this study, Heliotron E (a heliotron device with an $\ell = 2/m = 19$ helical coil, $R = 2.2$ m, $\langle a \rangle \approx 0.2$ m) was operated with the standard ($\beta^* = -0.185$) or the 2 cm inward shifted ($\beta^* = -0.192$) configuration at $|B| = 1.9$ T. Boronization by a 2.45 GHz ECH discharge is routinely performed for wall conditioning [9]. In order to reduce the rate of outgassing from the boronized wall, ECH discharge cleaning with helium gas was performed. In the plasma experiments, the plasma is initiated by ECH and sustained by ECH (ECH-only plasma) or NBI (NBI plasma). In some cases, ECH was superimposed during the NBI pulse (NBI + ECH plasma).

The T_e profile was measured by a multiple Thomson scattering system and an ECE radiometer. The n_e profile was measured by the Thomson scattering system or estimated from the line averaged electron density measured by a seven channel FIR interferometer. The T_i profile was mainly measured by a CXRS system using one of the NBI beamlines for the NBI or NBI + ECH cases. Therefore, information on the T_i profile for ECH-only plasmas was not obtained in this study. The plasma pressure profile was evaluated by using these density and temperature data. Neither the first particle pressure nor the impurity contribution was taken into account.

In order to survey the global characteristics of the obtained profiles, the peaking factors for the electron density, $n_e(0)/\langle n_e \rangle$, the electron and ion temperatures, $T_e(0)/\langle T_e \rangle$ and $T_i(0)/\langle T_i \rangle$, and the plasma pressure, $p(0)/\langle p \rangle$, are evaluated. Here, $x(0)$ is the central value of x and $\langle x \rangle$ denotes the volume average of x [10].

3. EFFECTS OF THE ECH POWER ABSORPTION PROFILE

Previously, the effect of off-axis heating was examined by using a 53 GHz ECH system with non-focused beams of TE_{02} wavegude mode and non-focused linearly polarized Gaussian beams in Heliotron E [11]. When the resonance layer was shifted to the high field side by decreasing the field strength on the magnetic axis from 1.9 to 1.76 T, the T_e profile became broad and the n_e profile was changed from hollow to broad. In this case,

however, the actual resonance position was vague since the beam was not focused and the expected single pass absorption rate was not so high. On the other hand, owing to its high single pass absorption rate, the 106 GHz second harmonic ECH with a well focused Gaussian beam has the potential for sophisticated local electron heating. By using this ECH system, the effect of the resonance position on the T_e profile and the global energy confinement was investigated in the Heliotron E device. Two methods were examined for changing the resonance position: tilting the beam direction in a poloidal cross-section, and shifting the injection angle in the toroidal direction. The global properties of the 106 GHz second harmonic ECH with normal injection are reported in Ref. [7].

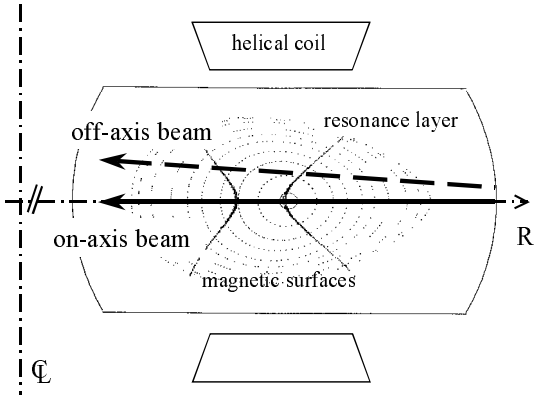

FIG. 1. Typical location of the ECH resonance layers in the poloidal cross-section at the ECH injection section.

3.1. Effect of Off-Axis Heating in the Case of Toroidally Perpendicular Injection

Figure 1 shows the location of resonance layers in the poloidal cross-section at the ECH launching section. The resonance position, where the ECH beam crosses a resonance layer, can be changed by tilting the beam direction in this poloidal cross-section without changing the strength of the confinement field. In order to realize this, the angle of the last focusing mirror was adjusted [12]. The shift of the resonance position is restricted to $r_{res}/a = 0.25$ owing to the limitation of the window size. The polarization of the launched waves was adjusted to obtain the best single pass absorption. The profiles of the field strength along the beam path for on- and off-axis cases are shown in FIG. 2.

Figure 3 shows the time traces of the major parameters ($\bar{n}_e$, H_α, T_e^{ECE} and P_{bol}) during an ECH pulse for (a) on-axis heating ($r_{res}/a = 0.05$, $P_{ECH} \approx 0.3$ MW) and (b) off-axis heating ($r_{res}/a = 0.25$, $P_{ECH} \approx 0.35$ MW) cases. The timings of the ECH pulse and gas puffing are also plotted in these figures. Figure 4 shows the T_e profile measured by Thomson scattering at the time denoted by the dashed line in FIG. 3. As shown in FIG. 3, for neither the on-axis nor the off-axis heating case was T_e^{ECE} saturated completely during the ECH pulse. However, its rate of increase is not high. Therefore, we consider that the profiles in FIG. 4 are close to the steady state.

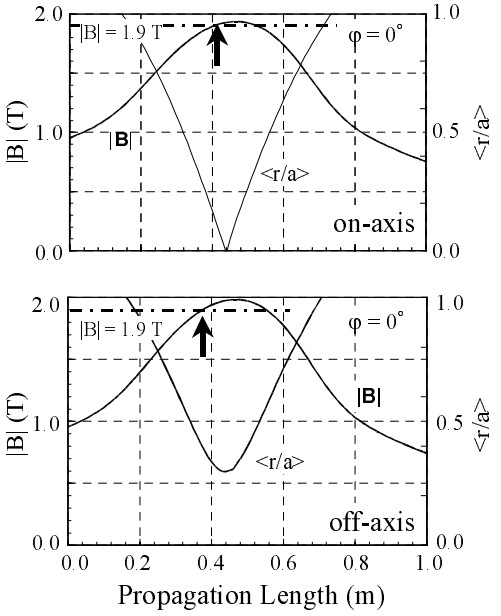

FIG. 2. Profile of the field strength along the beam path for on- and off-axis heating cases. ($\beta^* = -0.192$)

The position of maximum T_e position moved outward when the resonance position shifted outward, i.e. the T_e profile changed from peaked to hollow. The power deposition profile was evaluated experimentally from the decay time of T_e^{ECE}, the electron temperature from the ECE radiometer, for NBI + ECH combined heating plasmas (FIG. 8 in Ref. [7]). Although the experimental power deposition profile was broader

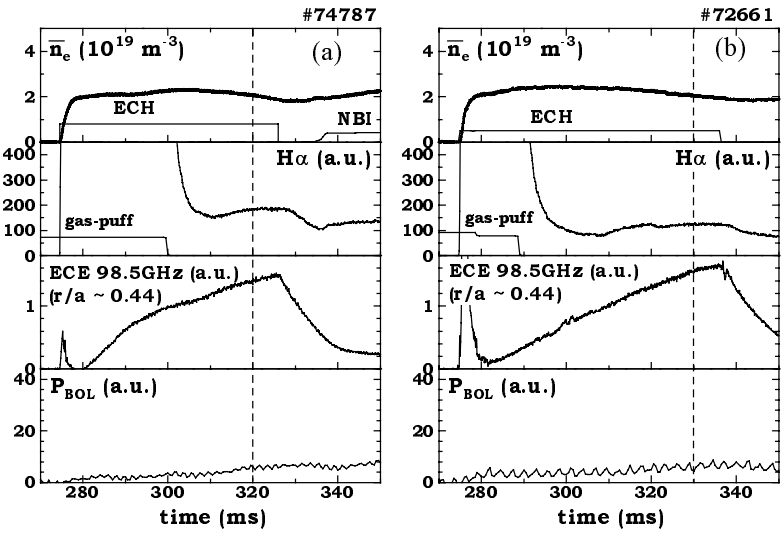

FIG. 3. Time traces of $\bar{n}_e$, H_α, T_e^{ECE} at $r/a \sim 0.44$ and P_{bol} for (a) the on-axis and (b) on-axis ECH cases. The timing of ECH pulse and gas puffing is also plotted. The plasma profile was measured at 320 and 330 ms for the cases in (a) and (b), respectively.

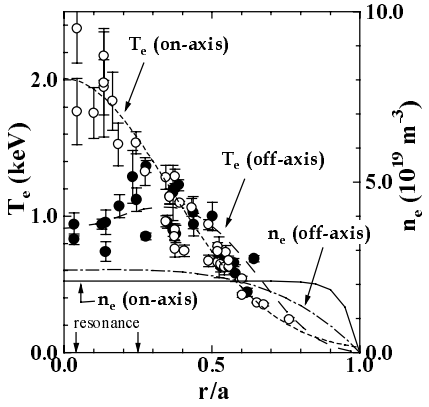

FIG. 4. Radial profiles of the electron temperature and density for the on- ($P_{ECH} \approx 0.3$ MW) and off-axis ($P_{ECH} \approx 0.35$ MW) heating cases. The resonance positions for each case are indicated.

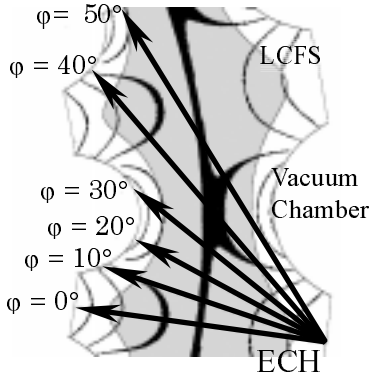

FIG. 5. Schematic view of the ECH beam path on the equatorial plane for oblique injection.

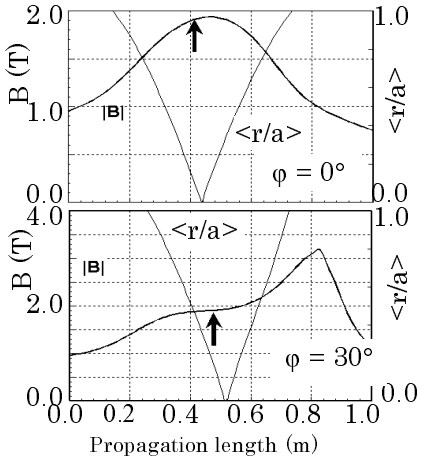

FIG. 6. Profile of the field strength along the beam path for oblique injection at φ = 0 °and 30 °.

than that of the ray tracing calculation, it was confirmed that the peak position of the absorbed power density moved outward in the off-axis heating case. Since there is no strong heat sink at the plasma centre, some outward non-diffusive (convection-like) heat flow should be required to explain the observed hollow T_e profile in the steady state. A simple analysis adding such a non-diffusive heat flow term in the electron heat transport equation indicates that this non-diffusive term has an important role in the core ($0 < r/a < 0.4$) transport [12]. It also indicates that the value of the flow increases approximately proportional to the minor radius in the core region. The cause of this non-diffusive outward heat flow and its relation to the particle pump-out phenomena are under investigation.

The electron density profile for ECH plasmas is usually flat, or sometimes hollow. However, the density profile has some dependence on the electron density and the heating power P_{ECH} (or the power density per unit volume, p_{ECH}). The value of $n_e(0)/\langle n_e \rangle$ tends to increase with $\bar{n}_e$ under the same range of P_{ECH} (FIG. 10 in Ref. [12]). The increase of P_{ECH} leads to a low $n_e(0)/\langle n_e \rangle$ for both on- and off-axis heating cases [7, 13]. The detailed mechanism of these phenomena is not clear, but it is considered that the production and loss of suprathermal electrons by ECH and the resultant electric field have an important role in the particle transport. The electron density profile for the same conditions as in FIG. 3 is also plotted in FIG. 4. Here the profile was evaluated from the FIR interferometer data. The effect of the ECH resonance position on the density profile was not so clear compared with the change of the T_e profile. The value of $n_e(0)/\langle n_e \rangle$ in the off-axis heating case was, however, larger than in the on-axis heating case for almost the same $\bar{n}_e$ and P_{ECH}. The low p_{ECH} in the central region for the off-axis case might explain this finding.

The electron stored energy evaluated from FIG. 4 was slightly higher in the on-axis heating case than in the off-axis heating case with almost the same range of $\bar{n}_e$ and P_{ECH}.

3.2. Oblique Injection Case

Oblique launching of an ECH beam in the toroidal direction was originally examined to study the possibility of plasma current control by ECH in heliotron devices [14]. The toroidal injection angle is controlled by changing the angle of the newly installed steering mirror at the injection port in the range $0° \le \varphi \le 50°$ (FIG. 5). Figure 6 shows variations of the magnetic field strength along the beam path for $\varphi = 0°$ and 30°. The profile of |B| along the beam path is drastically changed by changing the injection angle. The arrows in FIG. 6 indicate resonance points. The polarization angle of the microwaves was adjusted to couple the beam to the second harmonic X mode at the plasma edge in this experiment.

The single pass absorption profile of ECH power was evaluated by using a ray tracing calculation. With increasing φ, the absorption profile changes from a centre peaked profile to a broad profile with an outward shift of its maximum position. The actual absorption profile would be wider than the calculated one. The Doppler effect would make the absorption profile flater. The total single path absorption rate R_{abs}^{total} is expected to be almost 100% for all injection angles under the low-density condition of $\bar{n}_e \approx 1 \times 10^{19}$ m^{-3}. As the density increases, the refraction effect is enhanced, especially for larger φ cases. This causes a drastic drop in R_{abs}^{total} at the critical density depending on the injection angle. Owing to this feature, the density limit for the radiation collapse decreased with the increase of the injection angle [14].

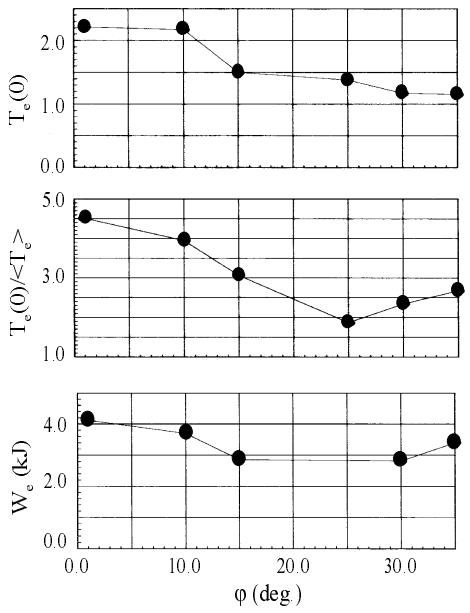

FIG. 7. Effect of injection angle φ on electron temperature $T_e(0)$ (typical error bar ±10–20%), its peaking parameter $T_e(0)/<T_e>$ and electron stored energy W_e.

Figure 7 shows the effect of the injection angle on the centre electron temperature $T_e(0)$, the electron temperature peaking factor $T_e(0)/<T_e>$, and the stored energy of the electrons W_e. The peaking factor was decreased from 4.5 to 1.8 by increasing φ. However, a hollow profile, which was found in the previous off-axis heating experiments, was not observed. The decrease of $T_e(0)/<T_e>$ is mainly due to the decrease of $T_e(0)$. At $\varphi \approx 30–35°$, $T_e(0)$ fell to almost half that of the perpendicular injection case, but $T_e(r/a = 0.5)$ was almost independent of the injection angle. In contrast to the previous off-axis heating case, the density profile was almost constant for the change of the injection angle in this oblique injection case.

The electron stored energy dropped by about 30% with increasing φ. This reduction is mainly caused by the difference in the T_e profile or the power deposition profile. Although the oblique launching of ECH has the potential to drive the non-inductive current (ECCD), the observed total ECCD current was less than 3–4 kA [14], which is too small to change the rotational transform or shear. Therefore, the change of the confinement condition by this current would be negligible.

Figure 8 shows the dependence of the T_e profile on the electron stored energy W_e for on-axis, off-axis and oblique ECH cases. As shown in this figure, the peaked T_e profile (or centre focused heating) had larger electron stored energy. This means that a peaked T_e profile is preferable for the global electron energy confinement of ECH plasmas if the total absorbed power is independent of the injection angle or the resonance position. From the ray tracing calculation, this condition is expected to be realized in this experiment. The existence of the radially increasing outward heat flow, discussed in Section 3.1, might be one of the reasons for the disadvantage of the off-centre (the off-axis or the oblique injection) heating.

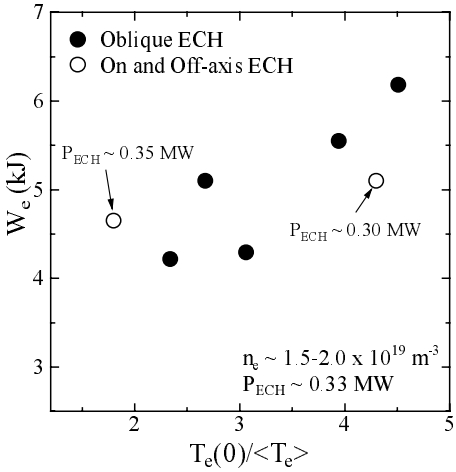

FIG. 8. T_e profile dependence on the electron stored energy for ECH-only plasmas.

It is well known that the radial electric field has an important effect on the transport in the rare collision regime for heliotron/stellarator devices. Recently, the ECH driven electron root feature was observed for ECH plasmas with a strongly peaked T_e profile in W7-AS [1]. The existence of strong positive E_r characterizes this operation mode. The experimental heat conductivity is much lower than the neoclassical value estimated under the $E_r = 0$ assumption. Positive E_r can be present also in our case. The value of E_r was consistent with the neoclassical calculation in the previous experiments with the 53 GHz ECH [11].

4. PROFILE EFFECTS ON THE GLOBAL ENERGY CONFINEMENT

4.1. Effects of the Heating Methods on Density and Temperature Profiles

In Heliotron E experiments with currentless plasmas, various profiles of the temperature and density have been obtained. The available ranges of these ratios are summarized in FIG. 9. Each parameter is calculated from the database for 1.0 MW $\lesssim P_{NBI}$(port through) $\lesssim$ 3.3 MW, 0.26 MW $\lesssim P_{ECH} \lesssim$ 0.4 MW, and the plasma parameters are 0.5 keV $\lesssim T_e \lesssim$ 2.3 keV, 0.3 keV $\lesssim T_i \lesssim$ 0.7 keV and 1.0×10^{19} $m^{-3} \lesssim \bar{n}_e \lesssim 6.7 \times 10^{19}$ m^{-3}. We omit the pellet injection cases in this survey owing to the lack of profile data, especially for the ion temperature. The ion temperature for ECH-only plasmas is also omitted for the same reason.

Figure 9 demonstrates the characteristics of ECH and NBI plasmas from the viewpoint of the radial profiles. The density profile of NBI plasmas mainly depended on the beam fuelling rate (NBI power) and the

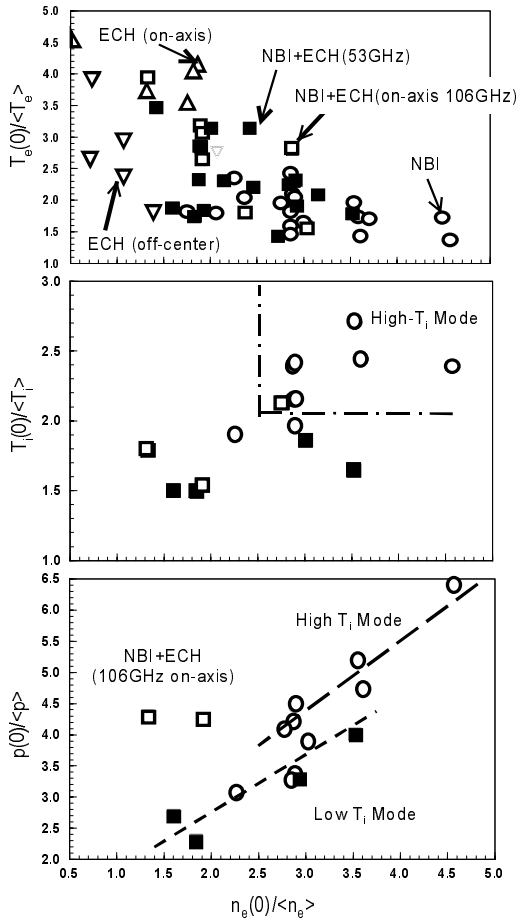

FIG. 9. Available range of peaking factors for n_e, T_e, T_i, and p. △: ECH (on-axis 106 GHz); ▽: ECH (oblique or off-axis 106 GHz); □: NBI + ECH (on-axis 106 GHz); ■: NBI + ECH (53 GHz); ○: NBI.

wall recycling. The wall recycling rate was changed by the wall conditioning after the boronization. In general, $\bar{n}_e$ for NBI plasmas gradually increased with time mainly owing to the beam fuelling effect. Therefore, most of the data in FIG. 9 were measured at near the time of maximum T_e. Examples of the power deposition profile for three different NBI plasmas are shown in FIG. 10: a high T_i mode NBI plasma, a low-T_i mode NBI plasma, a low T_i mode NBI + ECH plasma.

The density profile for NBI plasmas can be changed from broad to peaked, $1.2 \lesssim n_e(0)/<n_e> \lesssim 4.5$, while it is always very broad ($n_e(0)/<n_e> \lesssim 2$) for ECH-only plasmas. Basically this is explained as being due to the centre fuelling in the NBI case and to the particle pump-out in the ECH case. Particle pump-out also works for low-density NBI plasmas when an ECH pulse is superimposed [7]. It is interesting to note that highly peaked density profiles ($n_e(0)/<n_e> \gtrsim 4.0$) are obtained only for the high T_i mode NBI. Moreover, in the high T_i mode (FIG. 10(a)), the NBI power absorbed in the central region (propotional to the fuelling rate) is lower than in the low T_i mode (FIG. 10(b)), while $n_e(0)/<n_e>$ is almost the same for both cases. These observations would be related to the development of negative E_r in this mode [15].

The electron temperature profile for NBI plasmas is rather broad and almost unchanged ($1.3 \lesssim T_e(0)/<T_e> \lesssim 2.5$). The control of the ECH launching condition (on-axis, off-axis or oblique injection) greatly extends the $T_e(0)/<T_e>$ range, $1.8 \lesssim T_e(0)/<T_e> \lesssim 4.5$, in the low $\bar{n}_e$ region, although it cannot extend the available range of $T_i(0)/<T_i>$ and $n_e(0)/<n_e>$. A highly peaked T_e profile ($T_e(0)/<T_e> \gtrsim 3.5$) is attributed to the local on-axis heating by the 106 GHz ECH. Owing to this highly peaked T_e profile, the peaking factor of the pressure profile also increases when this ECH is superimposed onto low power NBI plasmas. In the high power NBI case, where $n_e(0)/<n_e>$ and $<n_e>$ are high, the ECH effect on the profile becomes weak. This is due to insufficient ECH power and/or the cut-off of the microwaves. A highly peaked T_e profile and a highly peaked n_e profile cannot be achieved simultaneously solely through the combination of NBI and ECH.

For the low T_i mode, there is little correlation between $n_e(0)/<n_e>$ and $T_i(0)/<T_i>$. The high T_i mode appears in the region of $n_e(0)/<n_e> \gtrsim 2.5$. For the high T_i mode plasmas, a positive correlation is observed between $n_e(0)/<n_e>$ and $T_i(0)/<T_i>$. It should be noted that the low T_i mode is also observed in the same range of $n_e(0)/<n_e>$ ($2.5 \lesssim n_e(0)/<n_e> \lesssim 3.5$) where the high T_i mode is available. This means that the high value of $n_e(0)/<n_e>$ is not a sufficient but a necessary condition for the high T_i mode.

The peakedness of pressure increases linearly with the density peakedness in both high T_i and low T_i modes. The data for the high

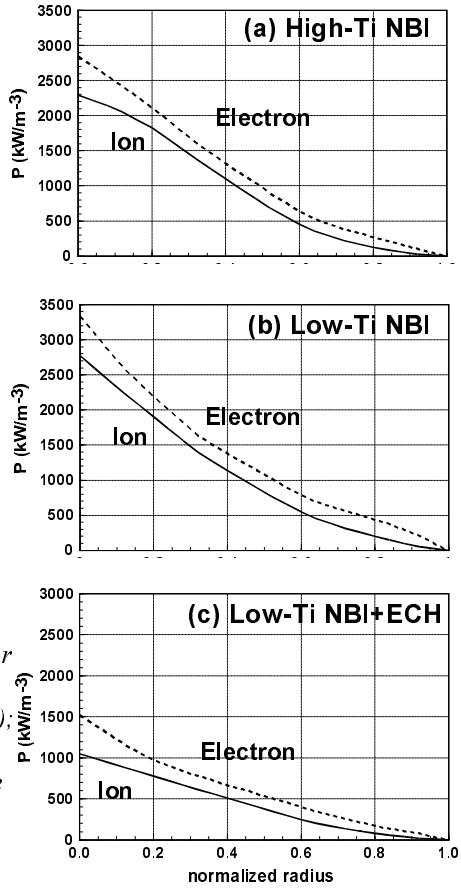

FIG. 10. Power deposition profiles for three types of discharge: (a) high T_i mode NBI plasma ($n_e(0)/<n_e> \sim 2.88$); (b) low T_i mode NBI plasma ($n_e(0)/<n_e> \sim 3.01$); (c) low T_i-mode NBI + ECH plasma ($n_e(0)/<n_e> \sim 1.91$).

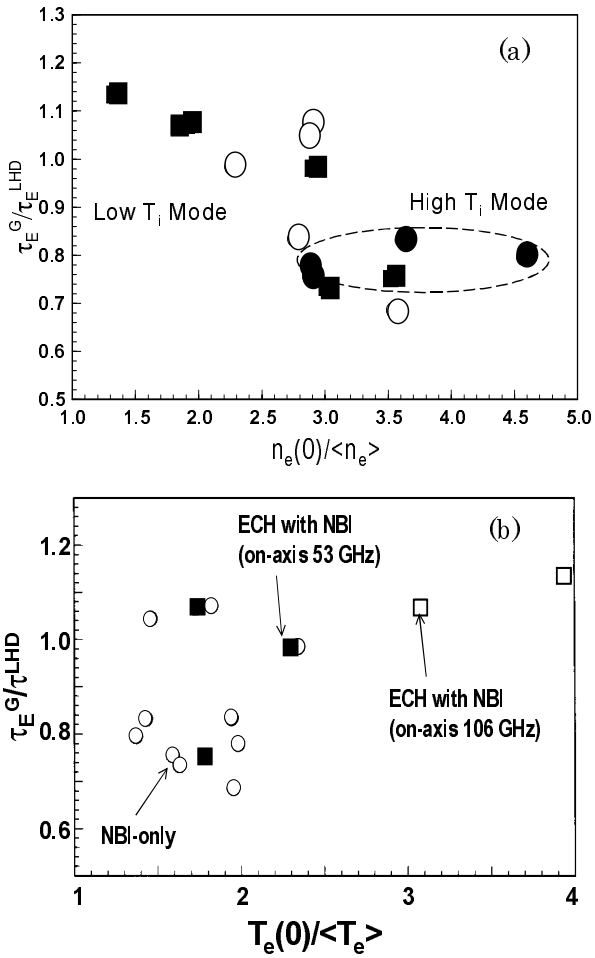

FIG. 11. (a) Relation of global energy confinement and density peaking factor.
○: NBI, ■: NBI + ECH, ●: high T_i mode NBI. (b) Relation of the global energy confinement and electron temperature peaking factor. ○: NBI, □: ECH on-axis (106 GHz) with NBI, ■: ECH (53 GHz) with NBI.

T_i mode are not an extension of the low T_i mode data. The data for the high T_i mode are located in the higher range of $p(0)/<p>$.

4.2. Profile Effects on the Global Energy Confinement

To study the profile effects on global energy confinement time τ_E^G, the LHD scaling τ_E^{LHD} [16] is used as the standard. This scaling is mainly based on Heliotron E data with rather broad density profiles. For the plasmas discussed in this article, the radiation loss measured by the bolometer is in the range of 10–30 % of the absorbed power. The dependence of this ratio of $P_{bol.}/P_{abs.}$ on $n_e(0)/<n_e>$ was weak and the radiation loss had no correlation with τ_E^G/τ_E^{LHD}. In the discussion on confinement, the dW/dt term was taken into account.

The normalized confinement time τ_E^G/τ_E^{LHD} for the low T_i and the high T_i modes is shown in FIG. 11(a) as a function of $n_e(0)/<n_e>$. (The vertical axis of this graph is expanded to clearly show the $n_e(0)/<n_e>$ dependence.) This figure covers a wider range of $n_e(0)/<n_e>$ than the original database of the LHD scaling. For the low T_i mode plasmas, τ_E^G is in the range predicted by τ_E^{LHD} when $n_e(0)/<n_e>$ is in the lower range. However, τ_E^G/τ_E^{LHD} decreases to ~70% with the increase of $n_e(0)/<n_e>$. It is considered that the increase of the centre value is not enough to compensate for the disadvantage of the peaked profile arising from 'the volume effect'. As for the high T_i mode, however, the degradation of the confinement with $n_e(0)/<n_e>$ is not observed. According to the transport analysis, the local ion heat conduction coefficient in the central region of high T_i mode plasmas is about one order lower than the low T_i mode with almost the same value of $n_e(0)/<n_e>$. This improvement in the central region is interpreted as being caused by the development of E_r or its shear [15]. However, since χ_e is almost the same for both cases, the electric field effect seems weak and not sufficient to improve the electron anomalous heat transport.

Since the range over which $T_e(0)/<T_e>$ can be varied is narrow for NBI plasmas, the dependence of τ_E^G/τ_E^{LHD} on $T_e(0)/<T_e>$ is less clear, as shown in FIG. 11(b). For the NBI + ECH case, which can provide a higher value of $T_e(0)/<T_e>$, the global energy confinement time seems to increase as $T_e(0)/<T_e>$. This dependence seems to be consistent with the findings described in Section 3, where W_e increased with $T_e(0)/<T_e>$ for ECH-only plasmas (FIG. 8). However, we should take care in reading this graph since only the data with 106 GHz on-axis ECH raise the τ_E^G/τ_E^{LHD} value. The $n_e(0)/<n_e>$ value of these data is located in the lowest region. The T_e profile dependence should be examined under a fixed density profile condition. In this experiment, however, $T_e(0)/<T_e>$ and $n_e(0)/<n_e>$ could not be controlled independently.

5. SUMMARY

In Heliotron E, the effects of the plasma profile on the confinement have been studied with special regard to the differences between heating methods (ECH, NBI, and NBI + ECH).

The controllability of the plasma profile by adjusting the heating conditions was examined. It was found that the control of the ECH launching condition was effective for controlling the T_e profile. The centre focused second harmonic X mode ECH produced a steep T_e profile of $T_e(0)/<T_e> \simeq 4.5$. A flat T_e profile of $T_e(0)/<T_e> \approx 1$ was produced by the off-centre ECH. With high power NBI, peaked electron density and ion temperature profiles were achieved simultaneously under the low recycling condition. However, the T_e profile was rather

broad in this case. The accessible ranges of the peaking parameters by using ECH, NBI and NBI + ECH without pellet fuelling were $0.5 \lesssim n_e(0)/\langle n_e \rangle \lesssim 4.5$, $1.4 \lesssim T_i(0)/\langle T_i \rangle \lesssim 2.7$, $1.3 \lesssim T_e(0)/\langle T_e \rangle \lesssim 4.5$ and $2.0 \lesssim p(0)/\langle p \rangle \lesssim 6.5$. In this scheme, however, it was difficult to control all parameters independently. A peaked T_i profile was obtained only by a peaked n_e profile, and the region of a highly peaked $T_e(r)$ with a highly peaked $n_e(r)$ was not accessible using this scheme only.

The relation between the peaking factors and the confinement was investigated. For ECH plasmas, the plasma with a peaked T_e profile has higher stored energy than plasma with a broad T_e profile for the same range of P_{ECH}. This finding suggests good electron transport in the central region of Heliotron E through the fine tuning of the local ECH.

For the low T_i mode NBI plasma, the global confinement time normalized by the LHD scaling, τ_E^G/τ_E^{LHD}, decreases as the density becomes peaked. By increasing $n_e(0)/\langle n_e \rangle$, the operation mode can be changed to the high T_i mode. For this high T_i mode, the $n_e(0)/\langle n_e \rangle$ dependence of τ_E^G/τ_E^{LHD} was weak. The confinement improvement of the high T_i mode is explained by the substantially reduced ion heat transport in the central region.

In conclusion, this study has revealed the following:

(1) A wide range of the peaking parameters ($0.5 \lesssim n_e(0)/\langle n_e \rangle \lesssim 4.5$, $1.4 \lesssim T_i(0)/\langle T_i \rangle \lesssim 2.7$, $1.3 \lesssim T_e(0)/\langle T_e \rangle \lesssim 4.5$ and $2.0 \lesssim p(0)/\langle p \rangle \lesssim 6.5$) was accessible for ECH and NBI heating experiments in Heliotron E without pellet injection. To expand this range, the strong particle pump-out induced by ECH must be overcome, and the mechanism of the 'consistency' of T_e profile for NBI plasmas should be studied.

(2) A high value of $n_e(0)/\langle n_e \rangle$ was a necessary condition for the high T_i mode. However, some other conditions are also required to enter the high T_i mode. It is necessary to study the prerequisite for the initial density (or pressure) profile to trigger the development of the radial electric field and its shear, which are the essential factors for the high T_i mode.

(3) To scale the global energy confinement of the helical plasmas in a wide range of $n_e(0)/\langle n_e \rangle$, the LHD scaling should be modified such that the profile effect is included in the scaling.

ACKNOWLEDGEMENT

This work was partially supported by the Collaboration Program of the Laboratory for Complex Energy Processes, Institute of Advanced Energy, Kyoto University.

REFERENCES

[1] KICK, M., et al., J. Plasma Fusion Res. SERIES, **1** (1998) 19.
[2] TUBBING, B. J. D., et al., Nucl. Fusion **31** (1991) 839.
[3] STRACHAN, J. D., et al., Phys. Rev. Lett. **58** (1987) 1004.
[4] SUDO, S., et al., J. Plasma Fusion Res. **69** (1993) 1208.
[5] OBIKI, T., et al., in Plasma Physics and Controlled Nuclear Fusion Research 1992 (Proc. 14th Int. Conf., Würzburg, 1992) **Vol. 2**, IAEA, Vienna (1993) 403.
[6] IDA, K., et al., in Fusion Energy 1996 (Proc. 16th Int. Conf. Montreal, 1996) **Vol. 2**, IAEA, Vienna (1997) 151.
[7] OBIKI, T., et al., ibid. p. 13.
[8] IDA, K, et al.,. J. Plasma Fusion Res. SERIES, **1** (1998) 239.
[9] KONDO, K. et al., J. Nucl. Mater. **220–222** (1995) 1052.
[10] OBIKI, T., et al., J. Plasma Fusion Res. SERIES **1** (1998) 27.
[11] OBIKI, T., et al., in Plasma Physics and Controlled Nuclear Fusion Research 1988 (Proc. 12th Int. Conf., Nice, 1988) **Vol. 2**, IAEA, Vienna (1989) 337.
[12] NAGASAKI, K., et al., J. Phys. Soc. Jpn. **67** (1998) 1625.
[13] ZUSHI, H., et al, "Density Clamping Phenomena in Electron Cyclotron Resonance Heated Plasma on Heliotron E", Res. Rep. **PPLK-R-27** (1988), Plasma Phy. Lab., Kyoto Univ.
[14] NAGASAKI, K., et al., in Controlled Fusion and Plasma Physics (Proc.. 25th Eur. Conf. Prague, 1998). **Vol. 22C**, European Physical Society, Geneva (1998).
[15] IDA, K., et al., Phys. Rev. Lett. **76** (1996) 1268.
[16] SUDO, S., et al., Nucl. Fusion **30** (1990) 11.